Author Manuscript

Author Manuscript

Author Manuscript

Author Manuscript

HHS Public Access

Author manuscript

Sci Transl Med. Author manuscript; available in PMC 2019 March 05.

Published in final edited form as:

Sci Transl Med. 2019 February 13; 11(479): . doi:10.1126/scitranslmed.aaq1427.

IDH1-R132H acts as a tumor suppressor in glioma via epigenetic upregulation of the DNA damage response

Felipe J. Núñez[1,2], **Flor M. Mendez**[2], **Padma Kadiyala**[1,2], **Mahmoud S. Alghamri**[1,2], **Masha G. Savelieff**[1,2,‡], **Maria B. Garcia-Fabiani**[1,2], **Santiago Haase**[1,2], **Carl Koschmann**[3], **Anda-Alexandra Calinescu**[1], **Neha Kamran**[1,2], **Rohin Patel**[1], **Stephen Carney**[1], **Marissa Z. Guo**[1], **Marta Edwards**[1], **Mats Ljungman**[4,5], **Tingting Qin**[6], **Maureen A. Sartor**[6], **Rebecca Tagett**[6], **Sriram Venneti**[7], **Jacqueline Brosnan-Cashman**[8], **Alan Meeker**[8], **Vera Gorbunova**[9], **Lili Zhao**[10], **Daniel M. Kremer**[11,12,13], **Li Zhang**[13], **Costas A. Lyssiotis**[11,13,14], **Lindsey Jones**[15], **Cameron J. Herting**[16,17], **James L. Ross**[16,18], **Dolores Hambardzumyan**[16], **Shawn Hervey-Jumper**[1,†], **Maria E. Figueroa**[7,19], **Pedro R. Lowenstein**[1,2,*], and **Maria G. Castro**[1,2,*]

[1]Department of Neurosurgery

[2]Department of Cell and Developmental Biology

[3]Department of Pediatrics

[4]Department of Radiation Oncology, University of Michigan Medical School, Ann Arbor, MI 48109, USA

[5]Department of Environmental Health Science, School of Public Health, University of Michigan, Ann Arbor, MI 48109, USA.

[6]Department of Computational Medicine and Bioinformatics, University of Michigan, Ann Arbor, MI 48109, USA

[7]Department of Pathology, University of Michigan Medical School, Ann Arbor, MI 48109, USA

[8]Departments of Pathology, Oncology and Urology, Johns Hopkins University, Baltimore, MD 21287, USA

[9]Department of Biology, University of Rochester, Rochester, NY 14627, USA

[10]Department of Biostatistics, University of Michigan Medical School, Ann Arbor, MI 48109

[11]Rogel Cancer Center, University of Michigan, Ann Arbor, MI, USA 48109.

[*]Corresponding author: mariacas@med.umich.edu or pedrol@med.umich.edu.

Author Contributions: F.J.N., P.R.L and M.G.C. conducted and designed experiments, analyzed data and manuscript writing. F.M.M., P.K., M. A., M.G.S., C.K., A-A.C N.K., N.K., R.P., S.C., M.Z.G., M.B.G., S.H., and M.E., performed experiments and data analysis. M.L. conducted Bru- seq analysis. T.Q and M. A. S. performed ChIP-seq analysis. R.T. performed RNA-seq analysis. J.B-C and A.M. performed ALT experiments. V.G. contributed with DNA repair reporter plasmids. L.Z. performed statistical analysis of the data. S.H-J. contributed to IHC analysis of human samples. D.M.K, L.Z., and C.A.L. evaluated 2HG concentration. C.J.H, J.L.R and D.H. generated glioma mouse models using the RCAS system. L.J. generated and characterized SF10602 human glioma cells. M.E.F. contributed to ChIP-seq experimental design and data analysis. P.R.L. and M.G.C. directed the research and generated the funding. All authors read and edited the manuscript.

Competing interests: Authors declare no competing interests.

Data and materials availability: All data associated with this study are in the paper or the Supplementary Materials. The RNA-seq datasets have been deposited in NCBI's Gene Expression Omnibus with identifiers GSE94902, GSE94974, and GSE94975.The ChiP-seq datasets have been deposited in NCBI's Gene Expression Omnibus with identifiers GSE99806. The materials generated in this study can be requested to M.G.C. without MTA.

Author Manuscript Author Manuscript Author Manuscript Author Manuscript

[12]Graduate Program in Chemical Biolgy, University of Michigan, Ann Arbor, MI, USA, 48109

[13]Department of Molecular and Integrative Physiology, University of Michigan, Ann Arbor, MI, USA 48109.

[14]Department of Internal Medicine, Division of Gastroenterology, University of Michigan, Ann Arbor, MI, USA 48109

[15]Department of Neurological Surgery, University of California, San Francisco, San Francisco, CA.

[16]Department of Pediatrics, Aflac Cancer and Blood Disorders Center, Children's Healthcare of Atlanta, Emory University School of Medicine, Atlanta, GA, USA.

[17]Graduate Division of Molecular and Systems Pharmacology, Emory University, Atlanta, GA, USA.

[18]Graduate Division of Cancer Biology, Emory University, Atlanta, GA, USA.

[19]Sylvester Comprehensive Cancer Center, University of Miami Miller School of Medicine, Miami, FL 33136-1000, USA.

‡Current address: SciGency Science Communications, Ann Arbor, MI 48104, USA

†Current address: Department of Neurosurgery, University of California, San Francisco, San Francisco, CA 94143, USA

Abstract

Glioma patients whose tumors carry a mutation in Isocitrate Dehydrogenase 1 ($IDH1^{R132H}$) are younger at diagnosis and live longer. *IDH1* mutations co-occur with other molecular lesions, such as 1p/19q co-deletion, inactivating mutations in the tumor suppressor protein 53 *(TP53)* gene, and loss of function mutations in alpha thalassemia/mental retardation syndrome X-linked gene *(ATRX).* All adult low-grade gliomas (LGGs) harboring ATRX loss also express the $IDH1^{R132H}$ mutation. The current molecular classification of LGGs is based, in part, on the distribution of these mutations. We modelled the molecular glioma subtype which harbors $IDH1^{R132H}$, and *TP53* and *ATRX* inactivating mutations. Previously, we established that ATRX deficiency, in the context of wt-IDH1, induces genomic instability, impairs non homologous end joining DNA repair, and increases sensitivity to DNA damaging therapies. In this study, we investigated the function of $IDH1^{R132H}$ in the context of TP53 and ATRX loss. We discovered that $IDH1^{R132H}$ expression in the genetic context of *ATRX* and *TP53* gene inactivation: (i) increases median survival (MS) in the absence of any treatment, (ii) enhances DNA damage response (DDR) via epigenetic upregulation of the Ataxia-telangiectasia mutated (ATM) signaling pathway, and (iii) elicits tumor radioresistance. Accordingly, pharmacological inhibition of ATM or checkpoint kinase 1 and 2 (CHK1/2), essential kinases in the DDR, restored the tumors' radiosensitivity. Translation of these findings to $IDH1^{132H}$ glioma patients harboring TP53 and ATRX loss, could significantly improve the therapeutic efficacy of radiotherapy, and consequently patient survival.

One sentence summary

Mutant IDH1 when co-expressed with inactivating TP53 and ATRX mutations in glioma, induces genomic stability and enhanced DNA repair, leading to resistance to genotoxic therapies.

Author Manuscript Author Manuscript Author Manuscript Author Manuscript

Introduction

Mutated isocitrate dehydrogenase 1 ($IDH1^{R132H}$) is found in 80 % of LGG (WHO grade II/III), and in a subset of high grade gliomas (WHO grade IV) (1, 2). Two main molecular subtypes of glioma, which harbor $IDH1^{R132H}$, have been identified expressing: i) $IDH1^{R132H}$, 1p/19q co-deletion, and *TERT* promoter mutations; and ii) $IDH1^{R132H}$, mutant *TP53,* and inactivation of *ATRX(*2, 3). In spite of a better prognosis, 50–75% of $IDH1^{R132H}$ gliomas undergo malignant transformation over time, becoming WHO grade IV glioblastomas (1, 4).

$IDH1^{R132H}$ has been identified as an early event in glioma development, preceding *TP53* and *ATRX* mutations (5, 6). $IDH1^{R132H}$ is a gain of function mutation that converts α-ketoglutarate to (*R*)-2- hydroxyglutarate (2HG) (7–9). 2HG inhibits DNA and histone-demethylases, namely the ten-eleven translocation enzymes (TETs) and lysine demethylases (KDMs) respectively, resulting in hypermethylation of DNA and histones (8, 9). This elicits epigenetic reprogramming of the $IDH1^{R132H}$ tumor cells' transcriptome (8–11). However, the molecular mechanisms which mediate increased survival in mIDH1 glioma patients remain unknown.

Genomic instability is prevalent in gliomas; it is thought to promote tumorigenesis and an aggressive phenotype (12, 13). DDR maintains genomic stability, senses DNA-damage, and regulates the mitotic cell cycle progression and DNA repair mechanisms (14). ATM, a member of PI3K-like protein kinase family, plays a critical role in these process (15).

Herein we demonstrate that $IDH1^{R132H}$, in the context of *ATRX* and *TP53* knock down (KD), increases DDR activity, enhancing genomic stability and extending MS in our mIDH1 mouse glioma model. We demonstrate that 2HG induces hypermethylation of histone 3 (H3) which elicits epigenetic reprogramming of the tumor cells' trancriptome. RNA-seq, Bru-seq, and ChIP-seq data from mIDH1 tumors uncovered enrichment of gene ontologies (GO) related to DDR, genomic stability, and activation of DNA repair pathways, i.e. ATM signaling and homologous recombination DNA repair (HR repair). Consequently, mIDH1 tumors exhibited enhanced DDR. Increases in DDR activity were observed in mIDH1 human glioma cells from surgical biopsies. Also, radiation failed to increase survival in the mIDH1 tumor-bearing animals. Pharmacological inhibition of DDR conferred radiosensitivity in mIDH1 tumor-bearing mice, leading to prolonged MS. Our findings highlight that DDR inhibition in combination with radiation could provide a novel therapeutic strategy for $IDH1^{R132H}$ glioma patients harboring *ATRX* and *TP53* inactivating mutations.

Results

Mutant IDH1 mouse glioma model exhibit increased survival and inhibition of oligodendrocyte differentiation

We generated a mIDH1 mouse glioma model using the Sleeping Beauty transposase system (13, 16) to uncover the impact of $IDH1^{R132H}$, in the context of ATRX and TP53 loss. Gliomas were induced by RTK/RAS/PI3K activation in combination with, shp53, shATRX

Author Manuscript Author Manuscript Author Manuscript Author Manuscript

and IDH1^{R132H} (fig. S1A). Mice from the three experimental groups namely: 1) control (NRAS GV12-shp53); 2) wt- IDH1 (NRAS GV12-shp53-shATRX) and 3) mIDH1 (NRAS GV12-shp53-shATRX-IDH1^{R132H}), developed brain tumors (fig. S1B) (Fig. 1A). The most aggressive tumor was wt-IDH1 (MS = 70 days). Notably, IDH1^{R132H} increased MS (163 days; $p < 0.0001$) (Fig. 1A). In all groups, tumor cells did not co-express myosin VIIa (fig. S1, C and D), indicating that they did not originate from cells in the ependymal layer of lateral ventricle. Due to the use of the shATRX construct to generate the wt-IDH1 and mIDH1 tumor models, ATRX expression was suppressed in these tumors (fig. S1E). IDH1^{R132H} expression was only positive in mIDH1 tumors (fig. S1F). Wt-IDH1 and mIDH1 tumors (fig. S1G) expressed p-ERK1/2, consistent with receptor tyrosine kinase (RTK) activation observed in human mIDH1 and wt-IDH1 gliomas (fig. S1, H to K). We generated neurospheres (NS) from mouse glioma sub-groups (fig. S2A). Both, wt-IDH1-NS and mIDH1-NS exhibited alternative lengthening of telomeres (ALT) which was associated with the presence of shATRX, whereas ALT was not detected in control NS or normal mouse brain (fig. S2B). IDH1^{R132H} expression was confirmed in mIDH1-NS (Fig. 1B), in human glioma cells stably transfected with IDH1^{R132H} (fig. S2C) and in human glioma cells with endogenous expression of IDH1^{R132H}, *TP53* and *ATRX* inactivating mutations (fig. S2D). In mIDH1-NS, 2HG concentration was on average 8.16 μg/mg of protein (μg/mg) (Fig. 1C). We observed a reduction in 2HG production in mIDH1- NS (~4-fold; $p < 0.0001$) after treatment with AGI-5198, an IDH1^{R132H} inhibitor; equivalent to the basal amount of wt-IDH1-NS (Fig. 1C). AGI-5198 inhibited cell viability (fig. S2E) and proliferation (2.8-fold; $p < 0.0001$) (fig. S2F) in mIDH1-NS consistent with previous results in human glioma cells (17). Earlier reports indicate that IDH1^{R132H} suppresses cellular differentiation (11, 17), thus, we evaluated the expression of oligodendrocyte and astrocyte differentiation markers. RNA-seq analysis revealed that a group of differentially expressed (DE) genes, involved in cell differentiation pathways, are downregulated in mIDH1 tumors (Fig. 1D and fig. S3A). GSEA analysis (Fig. 1F and fig. S3) suggests that IDH1^{R132H} inhibits differentiation in our model. Downregulated GO terms in mIDH1-NS include *Olig2* and *Mbp* (Fig. 1E, F and G). Mutant IDH1 tumors exhibited decreased amounts of: i) OLIG2 (2.3-fold; $p < 0.05$), ii) MBP (9.3-fold, $p < 0.001$); and iii) GFAP (6.7-fold; $p < 0.05$) (fig. S4A). Also, mIDH1 tumors exhibited increased SOX2 expression (fig. S4B) and equivalent expression of PAX3 (fig. S4C). In agreement with the in vivo data, wt-IDH1-NS expressed more OLIG2 than mIDH1-NS (fig. S4D). Inhibition of mIDH1 using AGI-5198 did not affect amounts of OLIG2 expression in wt-IDH1-NS, whereas it induced OLIG2 expression in mIDH1-NS (fig. S4D). The impact of mIDH1 on cell differentiation was confirmed in mIDH1-NS by immunofluorescence for OLIG2, GFAP and nestin; markers for oligodendrocytes, astrocytes and undifferentiated neural progenitor cells, respectively. Treatment of mIDH1-NS with AGI-5198 and retinoic acid enhanced OLIG2 and GFAP expression (fig. S4E).

We also investigated the tumor-initiating stem cell frequency using a limiting dilution assay (LDA). The LDA assay results indicate that both mouse NS and human mIDH1 glioma cells have lower stem cell frequency (fig. S5, A to J). In vivo analysis for tumor initiating cells (TICs) showed that 100% of animals generated tumors and succumbed due to tumor burden after implantation of 30×10^5, 10×10^5, 3×10^3 and 1×10^3 wt-IDH1 cells, whereas with mIDH1 cells, only 40% of animals generated tumors when implanted with 1×10^3 cells (fig.

Author Manuscript Author Manuscript Author Manuscript Author Manuscript

S5, K and L). These results suggest that there is a lower number of TICs among mIDH1 than among wt-IDH1 glioma cells. We also analyzed differences in the cell cycle profiles in our model in vivo. Frequency of mitotic ($pH3Ser10^+$) and actively proliferating (EdU^+) glioma cells was higher in wt-IDH1 tumors ($p < 0.0001$) (fig. S6A to F).

$IDH1^{R132H}$ induces H3 hypermethylation at genomic regions associated with DDR pathways

WB analysis in mIDH1-NS displayed increased amounts of H3K4me3 (1.9-fold; $p < 0.01$), H3K27me3 (2.3-fold; $p < 0.01$) and H3K36me3 (7.1-fold; $p < 0.01$) (Fig. 2A). Similar amounts of H3K4me1 (Fig. 2A) and H3K79me2 marks (fig. S7, A and B) were observed in all tumor genotypes. Mutant IDH1 tumor sections exhibited increased amounts of H3K27me3 (4.6-fold; $p < 0.001$) and H3K36me3 (7.3-fold; $p < 0.001$) (fig. S7C). There were no changes in mIDH1-NSH3 acetylation amounts (H3Kac) (fig. S7, D and E). H3 hypermethylation was also observed in human glioma cells harboring $IDH1^{R132H}$ (fig. S7F).

The impact of H3 hypermethylation on epigenetic reprogramming was assessed by ChIP-seq, and the differential enrichment of H3K4me3 and H3K27me3 was evaluated (Fig. 2, B to H). The heat-maps show differential peaks of histone marks centered at the peak midpoint in mIDH1-NS ($p < 1e\text{-}5$ as the cutoff) (Fig. 2, B and C, and fig. S7G). The average genomic distribution of H3K4me3 and H3K27me3 peaks in mIDH1-NS were around the transcription start sites (TSS) (fig. S7H). Identified peaks were annotated to genomic features (Fig. 2D). We observed increased amounts of differential peaks for H3 marks in mIDH1-NS at promoters, 5' UTRs and around the first exon (Fig. 2, E to H). Because these regions are generally linked to transcriptional regulatory elements, our findings indicate that $IDH1^{R132H}$ could participate in epigenetic reprogramming. We identified enriched GO terms linked to differential H3K4me3 and H3K27me3 peaks (Fig. 2I). Gene promoters enriched for H3K4me3 are generally associated with transcriptional activation. Differential GO terms enriched in our model included DDR, cell cycle control, and regulation of cell development (Fig. 2I). Usually, gene promoters enriched in H3K27me3 are associated with transcription repression, and differential GO terms included cell differentiation. This would imply that $IDH1^{R132H}$ prevents differentiation; in agreement with the RNA-seq and IHC results (Fig. 1, G to H, and fig. S4). Differential peaks for H3K4me3 around the promoter regions of BRCA1- associated ATM activator 1 *(Brat1)* and RAD51 associated protein 1 *(Rad51ap1),* which activate the HR repair pathway, were identified in mIDH1-NS suggesting upregulation of DDR mechanisms (Fig. 2, J and K).

$IDH1^{R132H}$ upregulates expression of the ATM signaling pathway

RNA-seq analysis identified 1973 DE genes, including upregulated genes related to "DNA damage stimulus responses" and "DNA repair" (fig. S8). GSEA indicated that DNA repair mechanisms were enriched in mIDH1-NS (FDR < 0.05) (Fig. 3, A and B). *Atm* (Figs. 1D, 3B and fig. S8) and *Brcal* (Fig. 1D, figs. S8, and S9) are key players in DNA repair and were shown to be DE in mIDH1-NS. This observation was mirrored in our enrichment maps showing biological functions involved in genomic stability: chromosome organization, DDR, DNA recombination and cell cycle checkpoints (Fig. 3B and fig. S9). *Fancd2, Rad50,*

Author Manuscript Author Manuscript Author Manuscript Author Manuscript

and *Rad51,* which are involved in DNA repair and DDR, were upregulated in mIDHl-NS (Fig. 1E and fig. S8).

WB analysis on NS demonstrated that ATM, BRCA1, FANCD2, RAD50 and RAD51 were increased in mIDHl-NS (Fig. 3C). In human glioma cells, $IDH1^{R132H}$ also increased expression of ATM and RAD51 (Fig. 3, D and E). IHC confirmed that RAD51, BRCA1, and ATM expression was enhanced in mIDH1 tumors, whereas p-DNA-PKcs protein expression, involved in non-homologous end-joining (NHEJ) repair, was not altered, and XRCC4 was decreased (fig. S10A). We validated these results by qPCR, observing increases in mRNA for *Atm* (2.8-fold; $p < 0.05$), *Brca1* (7.6-fold; $p < 0.01$), *Fancd2* (3.1-fold; $p < 0.01$) and *Rad51* (5.3-fold; $p < 0.01$) in mIDH1-NS (Fig. 3F). Moreover, using ChIP-qPCR, we found that H3K4me3, but not H3K27me3, was significantly enriched in mIDH1-NS versus wt-IDH1-NS for both *Atm* (1.8-fold; $p < 0.0001$) (Fig. 3G) and *Brca1*(2.2-fold; $p < 0.0001$) (Fig. 3H) genes around TSS.

Gene expression analysis suggested that $IDH1^{R132H}$ could enhance HR repair and DDR (Fig. 4A). Thus, we performed a functional DNA repair assay (Fig. 4B) in human glioma cells (Fig. 4C) and NS expressing wt-IDH1 or mIDH1 (Fig. 4D). Human and mouse mIDH1 glioma cells exhibited enhanced HR repair efficiency (SJGBM2: 3.4-fold, $p < 0.001$; MGG8: 1.8-fold, $p < 0.01$; mouse NS: 1.6-fold; $p < 0.01$) (Fig. 4, C and D). Treatment of wt-IDHl-NS with 2.5 mM of (2R)-Octyl- α-hydroxyglutarate (O-2HG), a cell permeable analogue of 2HG, enhanced HR repair efficiency (Fig. 4E).

We next quantified the kinetics of γH2AX and 53BP1 foci formation, in response to ionizing radiation (IR) (Fig. 4, F and G). The formation of γH2AX foci was increased ~2-fold versus basal quantities ($p < 0.0001$) 0.5 hours after IR in both wt-IDHl and mIDHl-NS, indicating DNA damage and DDR activation (Fig. 4F). At 4 hours after IR the number of foci in wt-IDHl-NS continued to increase (~2.5-fold; $p < 0.0001$), whereas in mIDHl-NS the foci number significantly decreased (~30%; $p < 0.0001$). At 48 hours, the number of foci in mIDH1 returned to basal foci number (Fig. 4F, and fig. S10B). Similarly, the average number of 53BP1 foci per cell increased at 0.5 hours after IR in both, wt-IDH1-NS and mIDH1-NS ($p < 0.0001$) (Fig. 4G). However, mIDH1-NS reached basal foci number before wt-IDH1-NS, indicating faster DSB repair. Additionally, we performed a neutral comet assay to assess genome integrity and DSB repair kinetics after IR (fig. S10C). IR immediately generated DNA damage characterized by increased nuclear tail lengths; proportional to the number of DSBs at neutral pH. Scores were proportionately higher (longer tails) for wt-IDH1, indicating greater DNA damage at earlier time points ($p < 0.05$) (fig. S10C).

We next studied the phosphorylation status of γH2AX, pCHK2, pRPA32 and pATM after IR. WB data showed a peak of γH2AX 0.5 hours after IR in wt-IDH1 and mIDH1 NS (Fig. 4H). However, the γH2AX signal decreased in mIDH1-NS at 4 hours after IR, compared to wt-IDH1-NS, indicating that mIDH1-NS repaired their DNA more efficiently (Fig. 4H). Similarly, pCHK2, pRPA32 and pATM signals decreased after 4 hours. In wt-IDH1 these signals remained positive 48 hours after IR (Fig. 4H). We also observed increased expression of total ATM in mIDH1-NS 4 hours after IR. Human glioma cells expressing

Author Manuscript Author Manuscript Author Manuscript Author Manuscript

IDH1^{R132H} displayed a similar pattern (Fig. 4I and fig. S10D and E). Our data shows that DNA repair efficiency is enhanced in mIDH1 tumor cells; in agreement with our RNA-seq and CHIP-seq analyses. (Figs. 1E and 2I). This was also assessed by Bru-seq analysis (Fig. 4J). Mutant IDH1-NS display higher transcription rate for *Atm* and *Rad50* (fold change >1.5) compared to wt-IDH1-NS (Fig. 4, K and L). Cell viability, evaluated after IR, was higher in mIDH1-NS versus wt-IDH1-NS (~2-fold; $p < 0.0001$) (Fig. 4M). Also, mIDH1-NS showed decreased NHEJ repair activity (fig. S10F), an error-prone DNA repair mechanism.

RAS pathway activation can confer radioresistance (18), thus we validated our results using NS generated from a mIDH1 glioma model independent of RAS activating mutations (19). Brain tumors were induced with RCAS PDGFB, mIDH1 or wt-IDH1, and shP53 in mixed background *NTva, Ink4a/Arf*$^{-/-}$ mice (19). We engineered the NS to encode shATRX in order to generate glioma cells with the following molecular alterations: PDGFB/shP53/shATRX/*Ink4a/Arf*$^{-/-}$/mIDH1 or PDGFB/shP53/shATRX/*Ink4a/Arf*$^{-/-}$/wt-IDH1. Using this model, we confirmed that mIDH1 confers radioresistance (~2-fold, $p < 0.0001$) (Fig. 4N). Likewise, human glioma cells harboring IDH1^{R132H} displayed higher viability in response to IR (2.3-fold; $p < 0.0001$) (Fig. 4O). These results were further validated in human glioma cells with endogenous expression of IDH1^{R132H} in the context of ATRX and TP53 inactivation (SF10602 and LC1035) which showed increased expression of RAD51 and ATM (fig. S11, A and B) and also displayed radioresistance (fig. S11 C and D). After treatment with AGI-5198, both mIDH1-NS and mIDH1 human glioma cells (Fig. 4M to O and fig. S11, E to G) became radiosensitive. In vitro radiosensitivity was also evaluated by clonogenic survival assay, with the survival dose response curve fitted to a linear regression (fig. S12 A to E). This experiment confirmed that mouse and human mIDH1 cells are less sensitive to radiation (fig. S12 C and D). The enhanced DDR in mIDH1 cells correlates with a faster digestion of chromatin, indicating that mIDH1 cells have a less condensed chromatin at a global level (fig. S13), which could facilitate recruitment of the DDR response machinery to DNA damage sites. Collectively, these results indicate that IDH1^{R132H} enhances DDR, imparting radioresistance independently of the presence of RAS activating mutations.

IDH1^{R132H} confers radioresistance in intracranial glioma models

To investigate the in vivo effects of mIDH1 in response to IR, we designed a pre-clinical trial using an intracranial glioma model, generated by implanting wt-IDH1-NS and mIDH1-NS into the brain of adult mice (Fig. 5A). At 7 days post implantation (DPI) with wt-IDH1-NS or mIDH1-NS, animals were treated with IR at the indicated doses. Untreated animals harboring wt-IDH1 tumors exhibited a MS = 21 days, which was increased after 20 Gy IR (MS = 51 days; $p = 0.0005$) (Fig. 5B). In contrast, animals harboring mIDH1 tumors exhibited MS = 33 days, which did not increase in response to IR (Fig. 5C). These results demonstrate that IDH1^{R132H} confers radioresistance in vivo. We then compared the genome-wide gene expression profiles, using RNA-seq after IR (Fig. 5, D to I). We examined the following animal groups: i) IR wt-IDH1 tumors (wt-IDH1-R) versus non-treated (NT) wt-IDH1 tumors (wt-IDH1-NT) (Fig. 5D), and ii) IR mIDH1 tumors (mIDH1- R) versus NT mIDH1 tumors (mIDH1-NT) (Fig. 5E). We found that the number of DE genes between mIDH1-R tumors and mIDH1-NT tumors increased at 20 Gy compared to 10 Gy (Fig. 5F).

Author Manuscript Author Manuscript Author Manuscript Author Manuscript

Wt-IDH1 tumors had fewer DE genes compared to mIDH1 tumors at both 10 Gy and 20 Gy (Fig. 5F). Also, wt-IDH1-R tumors did not exhibit an increase of DE genes between 10 Gy and 20 Gy (Fig. 5F). This suggests that in vivo resistance to radiation-induced DNA damage in mIDH1 glioma involves differential gene expression. Functionally, the upregulated genes in mIDH1 gliomas in response to IR are linked to regulation of cell proliferation, cell migration and cell homeostasis (Fig. 5G and H). Additionally, several genes involved in DNA repair were upregulated in mIDH1-R (Fig. 5I and fig S14), indicating that inducible DNA repair mechanisms were associated with in vivo radioresistance in the mIDHI glioma model. We analyzed the in vivo expression of Ki-67 (proliferation), CC3 (apoptosis) and γH2AX (DNA damage) at 14 and 21 DPI, in animals treated with 10 Gy, 20 Gy or NT (Fig. 5, A and J to N). In wt-IDH1-NT mice, we observed that Ki-67 (Fig. 5, J and L) was significantly decreased from 14 to 21 DPI ($>10^5$-fold; $p < 0.0001$), because the tumors had reached their maximum size, and tumor cells were no longer proliferating (Fig. 5O). Conversely, after 20 Gy, Ki-67 expression was enhanced ($>10^5$-fold; $p < 0.0001$), correlating with proliferating tumor cells. In mIDH1 mice we observed decreased Ki-67 at 21 DPI compared to 14 DPI, but no differences between the IR and NT groups (Fig. 5L), consistent with the lack of effect of IR on MS (Fig. 5C) and tumor size (Fig. 5P). CC3 was significantly higher in wt-IDH1-R at 14 and 21 DPI compared to the NT group ($>10^5$-fold; $p < 0.0001$) which correlated with a reduction in tumor size (Fig. 5, K and M). In mIDH1 tumors, CC3 expression was low in all experimental groups (Fig. 5, K and M) indicating no IR-mediated tumor cell death. Additionally, γH2AX increased in both, wt-IDH1 and mIDH1 tumors treated with 10 Gy and 20 Gy, indicative of DNA damage foci (Fig. 5N). However, in wt-IDH1 tumors, γH2AX was increased at 21 DPI versus 14 DPI (7.5-fold; $p < 0.01$), whereas in mIDH1 it decreased 4.5-fold ($p < 0.05$) at 21 DPI versus 14 DPI, implying better DNA repair activity (Fig. 5N). Taken together, these results suggest that $IDH1^{R132H}$ induces radioresistance in vivo by altering gene expression, enhancing DDR and DNA repair mechanisms.

Inhibition of DDR pathways restores radiosensitivity in mIDH1 glioma

The increased DDR and radioresistance observed in mIDH1 glioma suggest that pharmacological DDR inhibition could improve the response to IR. In vitro cell viability assays showed decreased sensitivity of mIDHl-NS to IR for both mouse glioma models (Fig. 6, A and B). We observed that Temozolamide (TMZ), which is standard of care of glioma patients, confers radiosensitivity in mIDHl-NS and mIDHI human glioma cells (fig. S15, A to C). Similarly, IR combined with specific inhibitors for ATM (KU60019) (Fig. 6, A and B) or CHK1/2 (AZD7762) (Fig. 6, C and D) decreased cell viability ($p < 0.0001$). Comparable results were observed in human glioma cells (fig. S15, D to I). To assess in vivo DDR inhibition in response to IR, we used the intracranial mIDHI model described above. Animals were treated with IR combined with KU60019 (Fig. 6E). Radiation or ATM inhibition alone did not modify MS compared to NT animals (Fig. 6F). However, KU60019 combined with IR improved MS of mIDHl mice (45 days) versus controls (MS = 30 days; $p < 0.01$) (Fig. 6F), consistent with decreased tumor size in mIDHl animals treated with 20 Gy and KU60019 (Fig. 6G). To study the effect of cell cycle progression in response to IR in mIDHl glioma, we combined IR with CHK1/2 inhibition in vivo (Fig. 6H). AZD7762 combined with IR significantly increased MS in mIDHl glioma-bearing mice (Fig. 6I).

Author Manuscript Author Manuscript Author Manuscript Author Manuscript

Tumor size was also significantly decreased in the IR + AZD7762 treated group at l4 DPI (5-fold; p < 0.000l) and 21 DPI (11-fold; p < 0.000l) (Fig. 6J). In wt-IDHl tumors ATM inhibition with IR did not improve MS compared to IR alone (fig. Sl5J). However, CHKl/2 inhibition with IR significantly increased MS in wt-IDHl glioma-bearing mice (fig. Sl5K). We also assessed CC3 expression in mIDH1 tumors after treatment with IR combined with KU600l9 or AZD7762 at l4 DPI (Fig. 6, K and L). CC3 expression is increased in mIDHl tumors treated with IR plus KU600l9 or AZD7762, suggesting that DDR inhibition in combination with IR induced apoptosis. In mIDHl human glioma cells, SFl0602 and LCl035, AZD7762 was able to revert radioresistance (Fig. 6 M and N). Consistent with our results, analysis of TCGA data-base indicated that LGG patients harboring IDHl^{Rl23H} with *TP53* and *ATRX* inactivating mutations have higher expression of *ATM* and *RAD50* mRNA than wt-IDH1 GBM (fig. S15, L and M), and higher *ATM* expression than wt-IDH1-LGG patients (fig. S15N). Additionally, the upregulation of *ATM* in glioma patients correlated with increased survival (fig. S15O).

Discussion

Patients harboring IDH1^{R132H} glioma exhibit longer MS (~6.6 years from diagnosis) compared with patients whose tumors express wt-IDH1 (~1.6 years from diagnosis) (1, 2, 20). In line with this, our mIDH1 mouse model exhibits increased median survival > 2-fold compared with wt- IDH1 tumors. It was reported (3) that the glioma subgroup harboring IDH1^{R132H}, ATRX, and TP53 loss also exhibits lengthening of telomeres. In our mouse glioma model telomere elongation is mediated by ALT (13, 21). Genomic stability in our mIDH1 glioma model is mediated via increased DDR due to epigenetic reprogramming of the tumor cells' transcriptome (fig. S16). DDR disruption is one of the hallmarks of gliomas and other cancers (22). ATM kinase senses DSB lesions on the DNA, activating responses that maintain genome integrity (23). Our ChIP-seq data revealed enrichment of H3K4me3 at promoter regions of genes involved in DDR and cell cycle progression. ChIP-qPCR showed enrichment of the H3K4me3 mark around *Atm* TSS, which would increase *Atm* expression. This was confirmed by Bru-seq and RNA-seq studies. Upregulation of *ATM* was also found in LGG patients harboring IDH1^{R132H} with *ATRX* and *TP53* gene inactivation; this correlates with an increased survival of these patients. We discovered that IDH1^{R132H} induced transcriptional activation of *Atm,* which resulted in efficient DNA repair activity via HR (24, 25). Because the chromatin was less condensed in mIDH1 glioma cells, this could enable the recruitment of the DDR machinery to sites of DNA damage.

Mutations in IDH1/2 are also detected in 15% of AML patients, which correlates with unfavorable prognosis (26). Intriguingly, ATM expression is downregulated (through H3K9me3) and DDR functions and genomic stability are also reduced in this setting (27). *AML-IDH1* mutant cells are more sensitive to chemotherapy and are highly malignant. Thus, the production of 2HG has opposite effects in these two different cancers. This highlights the critical influence of the genetic context in which IDH1^{R132H} acts. In the glioma subtype we studied, IDH1^{R132H} is expressed in the context of *TP53* and *ATRX* mutations, differing from AML, where *ATRX* gene inactivation is not present (26, 28).

Author Manuscript Author Manuscript Author Manuscript Author Manuscript

We hypothesized that the increase in DDR elicited by mIDH1 could induce radioresistance, because mIDH1 glioma cells are able to repair DNA damage inflicted by IR more efficiently. It appears that $IDH1^{R132H}$ induces genomic stability, which on one hand slows tumor growth, and on the other, increases DNA repair capacity, reducing the efficacy of radiotherapy. Previous studies used colon cancer cells, HeLa cells, and immortalized cells derived from high-grade gliomas suggest that $IDH1^{R132H}$ suppresses HR repair (29–32). None of these cells, however, originated from patient-derived $IDH1^{R132H}$ glioma, harboring concomitant mutations in *ATRX* and *TP53,* and no experiments were done orthotopically. These apparently opposing results reinforce the notion that the effects of $IDH1^{R132H}$ can vary according to tumor type/subtype and should be evaluated in an appropriate cellular and genetic context. Our results indicating that $IDH1^{R132H}$ decreases radiosensitivity and enhances DDR in glioma were validated in cells derived from glioma patients with endogenous expression of $IDH1^{R132H}$ in the context of TP53 and ATRX inactivation, and in a second mouse glioma model lacking *RAS* activating mutation (19). In agreement with our results, a recent study using gliomaspheres demonstrated that mIDH1 cultures are less sensitive to IR than wt-IDH1 cultures, however, this work does not distinguish between 1p/19q co-deleted and non-co-deleted mIDH1 glioma subtypes (33).

Thus, we postulated that inhibiting DDR would restitute glioma radiosensitivity in the mIDH1 glioma subtype under investigation. Indeed, when we blocked DDR, the tumors' sensitivity to IR therapy was restored (Fig. 6 and fig. S16). In patients, the effect of $IDH1^{R132H}$ on IR response remains controversial. Evidence in favor of $IDH1^{R132H}$ increasing or decreasing tumors' radiosensitivity has been published (20, 34–36). Glioma patients expressing $IDH1^{R132H}$ do live longer, but whether this is due to $IDH1^{R132H}$ tumors growing slower, or whether they are more radiosensitive has not yet been conclusively demonstrated. To conclusively demonstrate sensitivity to radiation in mIDH1 glioma patients, a control group not treated with radiation would be needed. Our in vivo results indicate that mIDH1 glioma-bearing mice do not exhibit a therapeutic response to IR. Our data also demonstrates that the effects mediated by $IDH1^{R132H}$ on DDR are dependent on the genetic context. This is in agreement with the only study available in the literature which included 300 LGG patients treated with or without radiotherapy (36). Similarly, survival of WHO II glioma patients expressing $IDH1^{R132H}$ treated with TMZ, was not further improved by radiotherapy (34). Also, a combination of vincristine, procarbazine, and lomustine WHO II glioma prolong overall survival compared with patients receiving IR alone (35), suggesting that tumors expressing $IDH1^{R132H}$ remain sensitive to chemotherapy, but not radiotherapy.

In conclusion, we discovered the mechanism by which $IDH1^{R132H}$, in the context of TP53 and ATRX inactivation, elicits epigenetic reprogramming of the ATM signaling pathway, which in turn increases DDR and genomic stability (fig. S16). Our data suggest a therapeutic strategy combining radiation with DDR inhibition to increase therapeutic efficacy in mIDH1 glioma patients.

Author Manuscript Author Manuscript Author Manuscript Author Manuscript

Material and methods

Study Design

To study the impact of IDH1^{R123H} activity in the contex of *TP53* and *ATRX*KD, we generated a genetically ingieneered animal model injecting Sleeping Beauty plasmids encoding NRAS-G12V, shp53, with or without shATRX, and with or without IDH1^{R132H} into the lateral ventricle of neonatal mice. Sample size and any data inclusion/exclusion were defined individually for each experiment. In addition, we used an intracranial animal model generated by implantation of glioma NS (wt-IDH1 and mIDH1) derived from our genetically ingieneered animal model to test theraupeutic responses. We also used an alternative model (PDGFB/shP53/shATRX/*Ink4a/Arf*$^{-/-}$ wtIDH1 or mIDH1 NS) which does not encode RAS activating mutations. We also used human glioma cells derived from patients harboring IDH1^{R132H} in the context of *TP53* and *ATRX* inactivating mutations, to confirm the results obtained from our animal models. Number of replicates are reported in the figure legends. Our studies were not randomized. We performed blinding for quantitative immunohistochemistry scoring. All RNA-seq and ChIP-seq data was deposited in public data-bases as is indicated in the respective sections. Material and methods are detailed in supplementary materials section.

Statistical analysis

All quantitative data is presented as the mean ± SEM from a least three independent samples. ANOVA and two-sample t tests were used for comparing a continuous outcome between groups. Survival curves were analyzed using the Kaplan-Meier method, and compared using Mantel-Cox tests; the effect size is expressed as median survival (MS). Significance is determined if $p < 0.05$. All analyses were conducted using GraphPad Prism software (version 6.01), SAS (version 9.4, SAS Institute, Cary, NC) or R (version 3.1.3). The statistical tests used are indicated in each figure legend.

Supplementary Material

Refer to Web version on PubMed Central for supplementary material.

Acknowledgments:

We thank Dr. Eric Holland for providing RCAS IDH1 R132H, RCAS IDH1 wild type plasmids (Fred Hutchinson Cancer Research Center and the University of Washington, Seattle); Dr. John Ohlfest (University of Minnesota, deceased) for providing the SB model plasmids; Dr. Joseph Costello, UCSF; and Drs. Hiro Wakimoto and Daniel Cahill, Harvard Medical School for providing mIDH1 human glioma cells, SF10602and MGG119 respectively. The content is solely the responsibility of the authors and does not necessarily represent the official views of the NIH.

Funding: Work supported by NIH/NINDS Grants, R37-NS094804, R01-NS105556 to M.G.C.; NIH/NINDS Grants R01-NS076991, and R01-NS096756 to P.R.L.; NIH/NIBIB: R01-EB022563; NIH/NCI U01CA224160; the Department of Neurosurgery and Leah's Happy Hearts to M.G.C. and P.R.L. RNA Biomedicine Grant F046166 to M L. and M.G.C.; NIH/NCI T32-CA009676 to S.C.; K08/NS099427 to C.K; NIH/NINDS-1F31NS103500 to F.M.M.; Aflac Cancer and Blood Disorders Center to D.H; NIH/NINDS F31NS106887 to C.H; University of Michigan's Program in Chemical Biology Graduate Assistance in Areas of National Need (GAANN) to D.M.K; 2017 AACR NextGen Grant for Transformative Cancer Research (17–20-01-LYSS) to C.A.L. Metabolomics studies supported by NIH grant DK097153, the Charles Woodson Research Fund, and the UM Pediatric Brain Tumor Initiative to C.A.L.-Dabbiere family, 5T32CA151022–07, and 5R01CA169316–05 to L.S.

Author Manuscript Author Manuscript Author Manuscript Author Manuscript

References and notes

1. Parsons DW et al., An integrated genomic analysis of human glioblastoma multiforme. Science 321, 1807–1812 (2008). [PubMed: 18772396]
2. N. Cancer Genome Atlas Research et al., Comprehensive, Integrative Genomic Analysis of Diffuse Lower-Grade Gliomas. The New England journal of medicine 372, 2481–2498 (2015). [PubMed: 26061751]
3. Ceccarelli M et al., Molecular Profiling Reveals Biologically Discrete Subsets and Pathways of Progression in Diffuse Glioma. Cell 164, 550–563 (2016). [PubMed: 26824661]
4. Leu S, von Felten S, Frank S, Boulay JL, Mariani L, IDH mutation is associated with higher risk of malignant transformation in low-grade glioma. J Neurooncol 127, 363–372 (2016). [PubMed: 26780338]
5. Watanabe T, Nobusawa S, Kleihues P, Ohgaki H, IDH1 mutations are early events in the development of astrocytomas and oligodendrogliomas. Am J Pathol 174, 1149–1153 (2009). [PubMed: 19246647]
6. Johnson BE et al., Mutational analysis reveals the origin and therapy-driven evolution of recurrent glioma. Science 343, 189–193 (2014). [PubMed: 24336570]
7. Dang L et al., Cancer-associated IDH1 mutations produce 2-hydroxyglutarate. Nature 462, 739–744 (2009). [PubMed: 19935646]
8. Xu W et al., Oncometabolite 2-hydroxyglutarate is a competitive inhibitor of alpha-ketoglutarate-dependent dioxygenases. Cancer Cell 19, 17–30 (2011). [PubMed: 21251613]
9. Figueroa ME et al., Leukemic IDH1 and IDH2 mutations result in a hypermethylation phenotype, disrupt TET2 function, and impair hematopoietic differentiation. Cancer Cell 18, 553–567 (2010). [PubMed: 21130701]
10. Turcan S et al., IDH1 mutation is sufficient to establish the glioma hypermethylator phenotype. Nature 483, 479–483 (2012). [PubMed: 22343889]
11. Lu C et al., IDH mutation impairs histone demethylation and results in a block to cell differentiation. Nature 483, 474–478 (2012). [PubMed: 22343901]
12. Vogelstein B et al., Cancer genome landscapes. Science 339, 1546–1558 (2013). [PubMed: 23539594]
13. Koschmann C et al., ATRX loss promotes tumor growth and impairs nonhomologous end joining DNA repair in glioma. Sci TranslMed 8, 328–328 (2016).
14. Jackson SP, Bartek J, The DNA damageresponse in human biology and disease. Nature 461, 1071–1078 (2009). [PubMed: 19847258]
15. Hanawalt PC, Historical perspective on the DNA damage response. DNA Repair (Amst) 36, 2–7 (2015). [PubMed: 26507443]
16. Wiesner SM et al., De novo induction of genetically engineered brain tumors in mice using plasmid DNA. Cancer Res 69, 431–439 (2009). [PubMed: 19147555]
17. Rohle D et al., An inhibitor of mutant IDH1 delays growth and promotes differentiation of glioma cells. Science 340, 626–630 (2013). [PubMed: 23558169]
18. Grana TM, Rusyn EV, Zhou H, Sartor CI, Cox AD, Ras mediates radioresistance through ough both phosphatidylinositol 3-kinase-dependent and Raf-dependent but mitogen-activated protein kinase/extracellular signal-regulated kinase kinase-independent signaling pathways. Cancer Res 62, 4142–4150 (2002). [PubMed: 12124353]
19. Amankulor NM et al., Mutant IDH1 regulates the tumor-associated immune system in gliomas. Genes Dev 31, 774–786 (2017). [PubMed: 28465358]
20. Yan H et al., IDH1 and IDH2 mutations in gliomas. NEngl JMed 360, 765–773 (2009).
21. Heaphy CM et al., Altered telomeres in tumors with ATRX and DAXX mutations. Science 333, 425 (2011). [PubMed: 21719641]
22. Godek KM et al., chromosomal omosomal Instability Affects the Tumorigenicity of Glioblastoma Tumor- Initiating Cells. Cancer discovery 6, 532–545 (2016). [PubMed: 27001151]

Author Manuscript Author Manuscript Author Manuscript Author Manuscript

23. Xu Y et al., Targeted disruption of ATM leads to growth retardation, chromosomal fragmentation during meiosis, immune defects, and thymic lymphoma. Genes & development 10, 2411–2422 (1996). [PubMed: 8843194]
24. Tubbs A, Nussenzweig A, Endogenous DNA Damage as a Source of Genomic Instability in Cancer. Cell 168, 644–656 (2017). [PubMed: 28187286]
25. Serrano L et al., Homologous recombination conserves DNA sequence integrity throughout oughout the cell cycle in embryonic stem cells. Stem Cells Dev 20, 363–374 (2011). [PubMed: 20491544]
26. Paschka P et al., IDH1 and IDH2 mutations are frequent genetic alterations in acute myeloid leukemia and confer adverse prognosis in cytogenetically normal acute myeloid leukemia with NPM1 mutation without FLT3 internal tandem duplication. J Clin Oncol 28, 3636–3643 (2010). [PubMed: 20567020]
27. Inoue S et al., Mutant IDH1 Downregulates ATM and Alters DNA Repair and Sensitivity to DNA Damage Independent of TET2. Cancer Cell 30, 337–348 (2016). [PubMed: 27424808]
28. Patel JP et al., Prognostic relevance of integrated genetic profiling in acute myeloid leukemia. The New England journal of medicine 366, 1079–1089 (2012). [PubMed: 22417203]
29. Molenaar RJ et al., Radioprotection of IDH1-Mutated Cancer Cells by the IDH1-Mutant Inhibitor AGI- 5198. Cancer Res 75, 4790–4802 (2015). [PubMed: 26363012]
30. Sulkowski PL et al., 2-Hydroxyglutarate produced by neomorphic IDH mutations suppresses homologous recombination and induces PARP inhibitor sensitivity. Sci TranslMed 9, (2017).
31. Li S et al., Overexpression of isocitrate dehydrogenase mutant proteins renders glioma cells more sensitive to radiation. Neuro Oncol 15, 57–68 (2013). [PubMed: 23115158]
32. Kessler J et al., IDH1(R132H) mutation causes a less aggressive phenotype and radio sensitizes human malignant glioma cells independent of the oxygenation status. Radiother Oncol 116, 381–387 (2015). [PubMed: 26328938]
33. Garrett M et al., Metabolic characterization of isocitrate dehydrogenase (IDH) mutant and IDH wildtype gliomaspheres uncovers cell type-specific vulnerabilities. Cancer Metab 6, 4 (2018). [PubMed: 29692895]
34. Wahl M et al., Chemotherapy for adult low-grade gliomas: clinical outcomes by molecular subtype in a phase II study of adjuvant temozolomide. Neuro-oncology 19, 242–251 (2017). [PubMed: 27571885]
35. Buckner JC et al., Radiation plus Procarbazine, CCNU, and Vincristine in Low-Grade Glioma. NEngl J Med 374, 1344–1355 (2016).
36. Karim AB et al., Randomized trial on the efficacy of radiotherapy for cerebral low-grade glioma in the adult: European Organization for Research and Treatment of Cancer Study 22845 with the Medical Research Council study BRO4: an interim analysis. Int JRadiat Oncol Biol Phys 52, 316–324 (2002). [PubMed: 11872276]
37. Hambardzumyan D, Amankulor NM, Helmy KY, Becher OJ, Holland EC, Modeling Adult Gliomas Using RCAS/t-va Technology. Transl Oncol 2, 89–95 (2009). [PubMed: 19412424]
38. Herting CJ et al., Genetic driver mutations define the expression signature and microenvironmental composition of high-grade gliomas. Glia 65, 1914–1926 (2017). [PubMed: 28836293]
39. Wakimoto H et al., Targetable signaling pathway mutations are associated with malignant phenotype in IDH-mutant gliomas. Clin Cancer Res 20, 2898–2909 (2014). [PubMed: 24714777]
40. Wakimoto H et al., Maintenance of primary tumor phenotype and genotype in glioblastoma stem cells. Neuro Oncol 14, 132–144 (2012). [PubMed: 22067563]
41. Hu Y, Smyth GK, ELD A: extreme limiting dilution analysis for comparing depleted and enriched populations in stem cell and other assays. J Immunol Methods 347, 70–78 (2009). [PubMed: 19567251]
42. Seluanov A, Mao Z, Gorbunova V, Analysis of DNA double-strand break (DSB) repair in mammalian cells. J Vis Exp, (2010).
43. Henson JD et al., DNA C-circles are specific and quantifiable markers of alternative-lengthening-of- telomeres activity. Nat Biotechnol 27, 1181–1185 (2009). [PubMed: 19935656]

Author Manuscript Author Manuscript Author Manuscript Author Manuscript

44. Subramanian A et al., Gene set enrichment analysis: a knowledge-based approach for interpreting genome- wide expression profiles. Proc Natl Acad Sci U S A 102, 15545–15550 (2005). [PubMed: 16199517]

45. Efron B, Tibshirani R, On Testing the Significance of Sets of Genes. Annals of Applied Statistics 1, 107–129 (2007).

46. Paulsen M et al. Use of Bru-Seq and BruChase-Seq for genome-wide assessment of the synthesis and stability of RNA. Methods (San Diego, Calif). 67, 45–54 (2014).

47. Cavalcante RG, Sartor MA, annotatr: Genomic regions in context. Bioinformatics, (2017).

48. Cavalcante RG et al., Broad-Enrich: functional interpretation of large sets of broad genomic regions.Bioinformatics 30, i393–400 (2014). [PubMed: 25161225]

Author Manuscript Author Manuscript Author Manuscript Author Manuscript

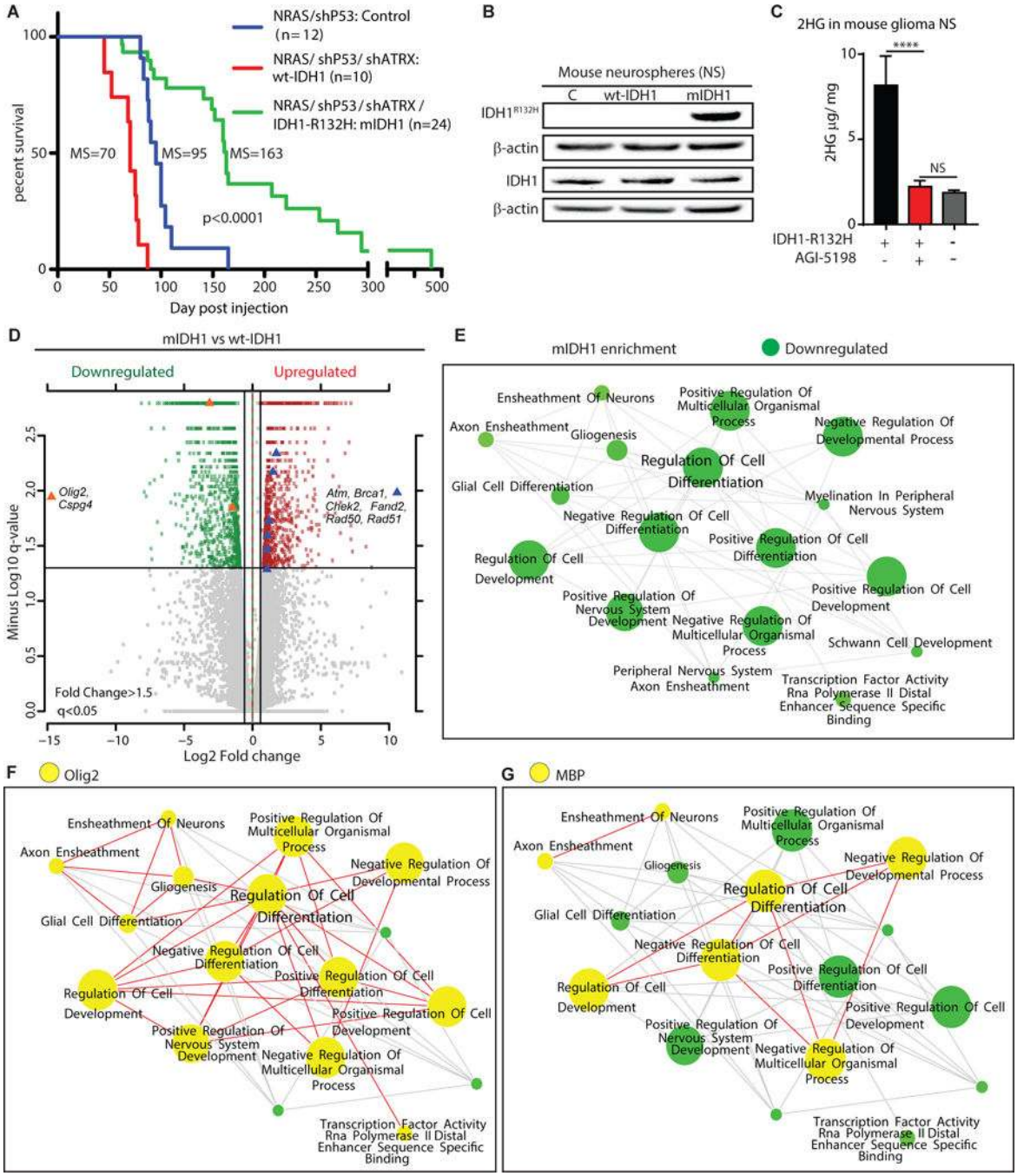

Figure 1. IDH1^{R132H} increases median survival and inhibits cell differentiation in a mouse glioma model

(**A**) Kaplan-Meier survival curves for mice bearing mIDH1 (n = 24), wt-IDH1 (n = 10) or control (n = 12) gliomas ($p < 0.0001$, Mantel-Cox test). MS: median survival.

(**B**) WB using NS from control (c), wt-IDH1 and mIDH1 tumors. Data shown as IDH1^{R132H} and total IDH1 expression. β-actin and vinculin: loading controls.

Author Manuscript Author Manuscript Author Manuscript Author Manuscript

(**C**) 2HG expression in mouse NS in the presence or absence of 1.5μM of AGI-5198. ****p < 0.0001; NS = non-significant; unpaired t-test. Data shown as mean ± SEM (n = 3 biological replicates).

(**D**) Differential gene expression in mIDH1 tumors analyzed by RNA-seq. Volcano plot comparing DE genes in mIDH1 versus wt-IDH1 mouse NS. The −log10 q-values were plotted against the log2 Fold-Change (FC) in gene expression. Upregulated genes (n = 906; ≥1.5-fold; FDR corrected p- value < 0.05) are depicted as red dots; genes that were downregulated (n = 1067 ≥1.5-fold; FDR corrected p-value < 0.05) are depicted as green. Orange symbols represent downregulated genes involved in oligodendrocyte differentiation. Blue symbol represent upregulated genes involved in DDR. FDR corrected p-values = q-values; two-sided moderated Student's t-test (n = 3 biological replicates per group).

(**E-G**) Pathway enrichment map of DE genes in mIDH1 versus wt-IDH1-NS. Clusters of nodes depicted in green (E) illustrate differentially downregulated pathways resulting from GSEA (p < 0.05, overlap cutoff > 0.5) (full map in Fig. S4). The yellow highlighted nodes indicate downregulated GO terms containing *Olig2* (F) and *Mbp* (G).

Author Manuscript Author Manuscript Author Manuscript Author Manuscript

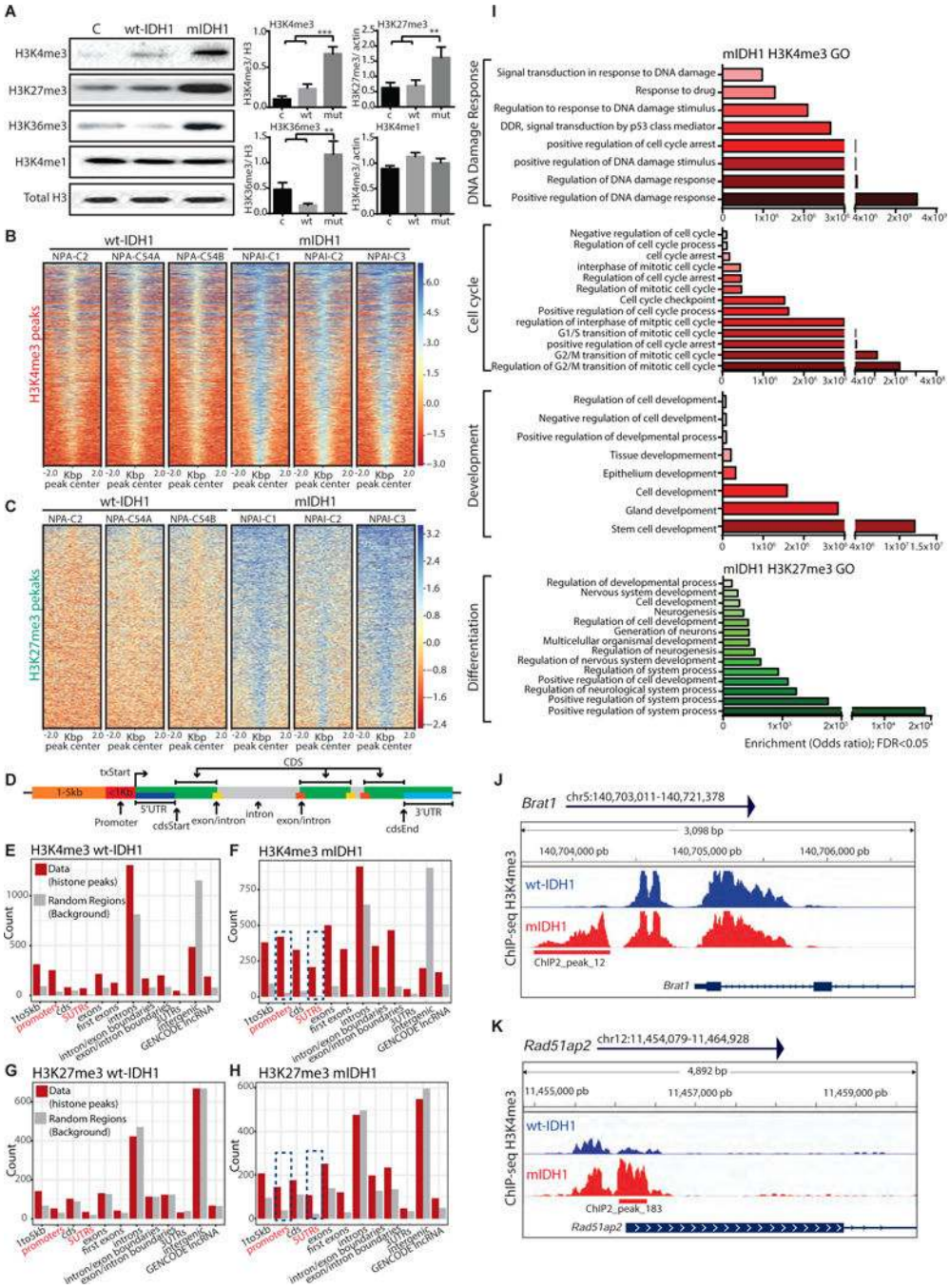

Figure 2. IDH1^{R132H} increases histone hypermethylation and elicits epigenetic enrichment of gene ontologies related to DDR

(**A**) WB assay performed on control (C), wt-IDH1-NS and mIDH1-NS for H3K4me3, H3K27me3, H3K36me3, H3K4me1 marks. Total histone H3: loading control. The bar graph represents the semi-quantification of the histone bands (n = 3 technical replicates). **p < 0.01; one-way ANOVA.

(**B-C**) ChIP-seq enrichment across the genome shows differential peaks of histone marks in mIDH1-NS. Heat-maps show H3K4me3 (B) and H3K27me3 (C) peaks ± 2 Kbp with each

Author Manuscript Author Manuscript Author Manuscript Author Manuscript

row representing a distinct peak. The blue to red color gradient indicates high to low counts in the corresponding region. The maps show biological replicates per group (n = 3) for wt-IDH1-NS and mIDH1-NS.

(**D-H**) Distribution of histone marks within specific genomic regions. (D) Diagram represents known genome annotations. (E, F) Bar graphs represent the specific genomic regions where the H3K4me3 is enriched in wt-IDH1-NS (E) and mIDH1-NS (F). (G, H) Bar graphs represent the specific genomic regions where H3K27me3 is enriched in wt-IDH1-NS(G) and mIDH1-NS (H). Red bars show ChIP-seq data and gray bars shows random regions as background. The y axis represents the total number of marks present in each category. Blue dashed lines in F and H, indicate promoter and 5' UTR regions.

(**I**) Genes enriched in H3K4me3 or H3K27me3 marks are linked to distinct functional GO terms by ChIP-seq analysis. Genes enriched in H3K4me3 or H3K27me3 marks are linked to distinct functional GO terms by ChIP-seq analysis. Bar graphs represent GO terms containing genes that have enrichment of the H3K4me3 mark (red scale) or the H3K27me3 mark (green scale) at their promoter regions in mIDH1 tumor NS. The GO terms significance was determined by false discovery rate (FDR < 0.05) and enrichment is expressed as odds ratio.

(**J, K**) H3K4me3 occupancy in specific genomic regions of DNA repair regulatory genes *Brat1*. (J) and *Rad51ap2* (K). The y axis of each profile represents the estimated number of immunoprecipitated fragments at each position normalized to the total number of reads in a given dataset. RefSeq gene annotations are shown. Differential peaks (FDR < 0.05) in mIDH1-NS are represented in red compared to wt-IDH1-NS in blue (n = 3 biological replicates per group).

Author Manuscript Author Manuscript Author Manuscript Author Manuscript

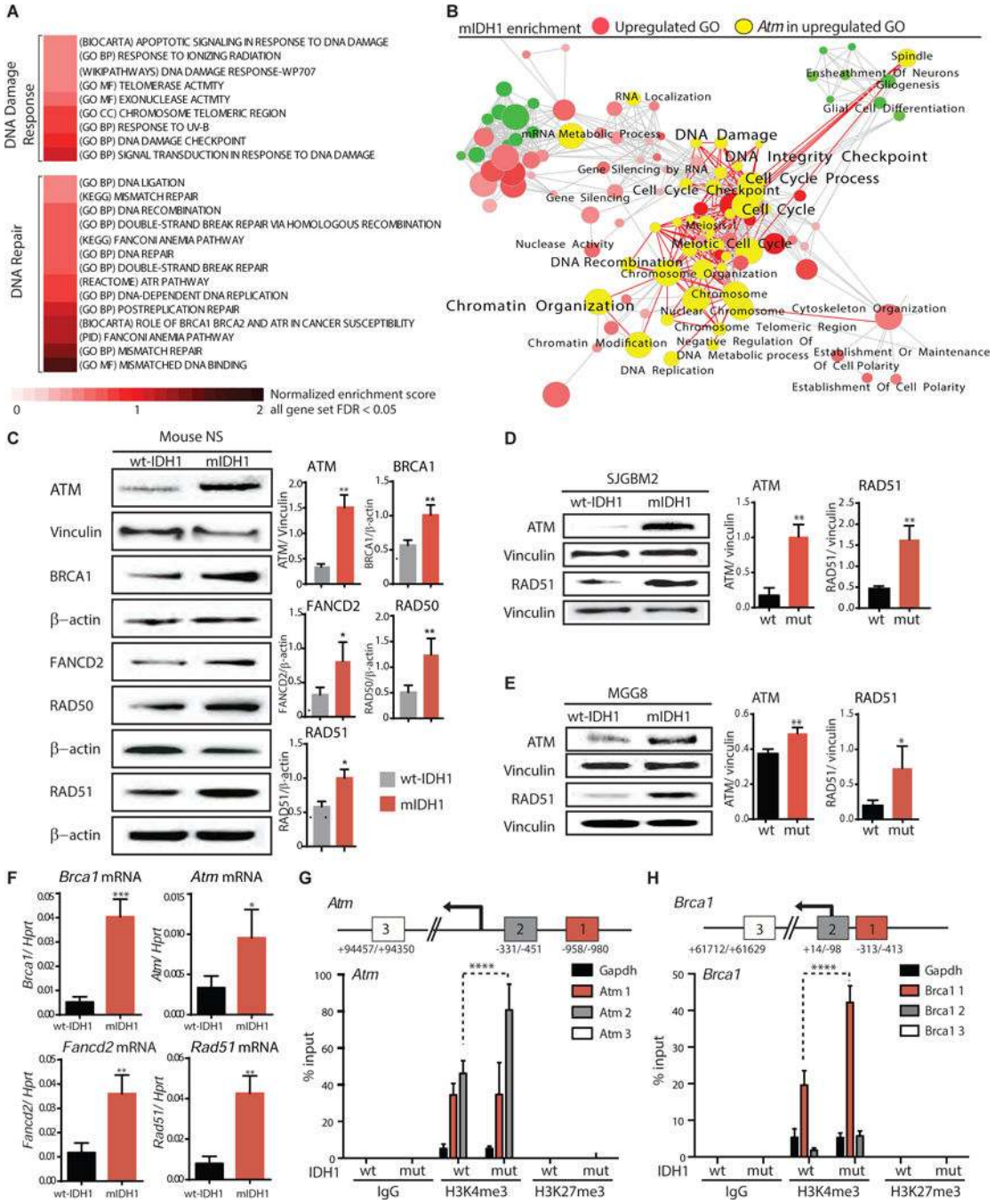

Figure 3. IDH1^{R132H} upregulates ATM signaling in the context of ATRX and TP53 KD

(**A**) GSEA of transcriptional changes comparing with mIDH1-NS versus wt-IDH1-NS. Positive normalized enrichment scores (red scale; FDR < 0.05) show GO terms linked to DDR and DNA repair pathways that are enriched in mIDH1-NS.

(**B**) Pathway enrichment map of DE genes in mIDH1-NS versus wt-IDH1-NS. Clusters of red nodes illustrate differential enrichment (upregulation) in mIDH1-NS ($p < 0.05$, overlap cutoff > 0.5) and they were extracted from the GSEA results comparing mIDH1-NS versus

Author Manuscript Author Manuscript Author Manuscript Author Manuscript

wt-IDH1-NS (fig. S4). The yellow highlighted circles indicate nodes containing *Atm* in upregulated GO terms.

(**C**) Expression of ATM, BRCA1, FANCD2, RAD50 and RAD51 in mouse NS. WB analysis using wt-IDH1-NS and mIDH1-NS. β-actin: loading control. Bar graph represents semi-quantification of WB assay (n = 3). *p < 0.05; **p < 0.01; one-way ANOVA. Data shown as ± SEM (n = 3 technical replicates).

(**D, E**) WB for ATM and RAD51 performed on wt-IDH1 and mIDH1 SJGBM2 (D) and MGG8 (E) human glioma cells. Vinculin: loading control. Bar graph represents semi-quantification of WB assay (n = 3). *p < 0.05; **p < 0.01; ***p < 0.001; one-way ANOVA. Bars represent mean ± SEM (n = 3 technical replicates).

(**F**) mRNA expression of DNA repair genes *Brca1, Atm, Fancd2* and *Rad51* in wt-IDH1 and mIDH1-NS. RT-qPCR data are expressed relative to *Hprt* gene. *p < 0.05; **p < 0.01; ***p < 0.001; unpaired t-test. Data shown as mean ± SEM (n = 3 technical replicates).

(**G-H**) ChIP-qPCR for *Atm* (G) and *Brca1* (H) was performed on isolated chromatin from wt-IDH1 and mIDH1-NS, immunoprecipitated with H3K4me3 and H3K27me3 antibodies. Diagram of *Atm* and *Brca1* genomic regions, indicating the qPCR primer positions (1, 2 and 3). Bar graphs show histone mark enrichment in the indicated genomic region. Data is expressed in % input. ****p < 0.0001; two-way ANOVA (n = 3 technical replicates).

Author Manuscript Author Manuscript Author Manuscript Author Manuscript

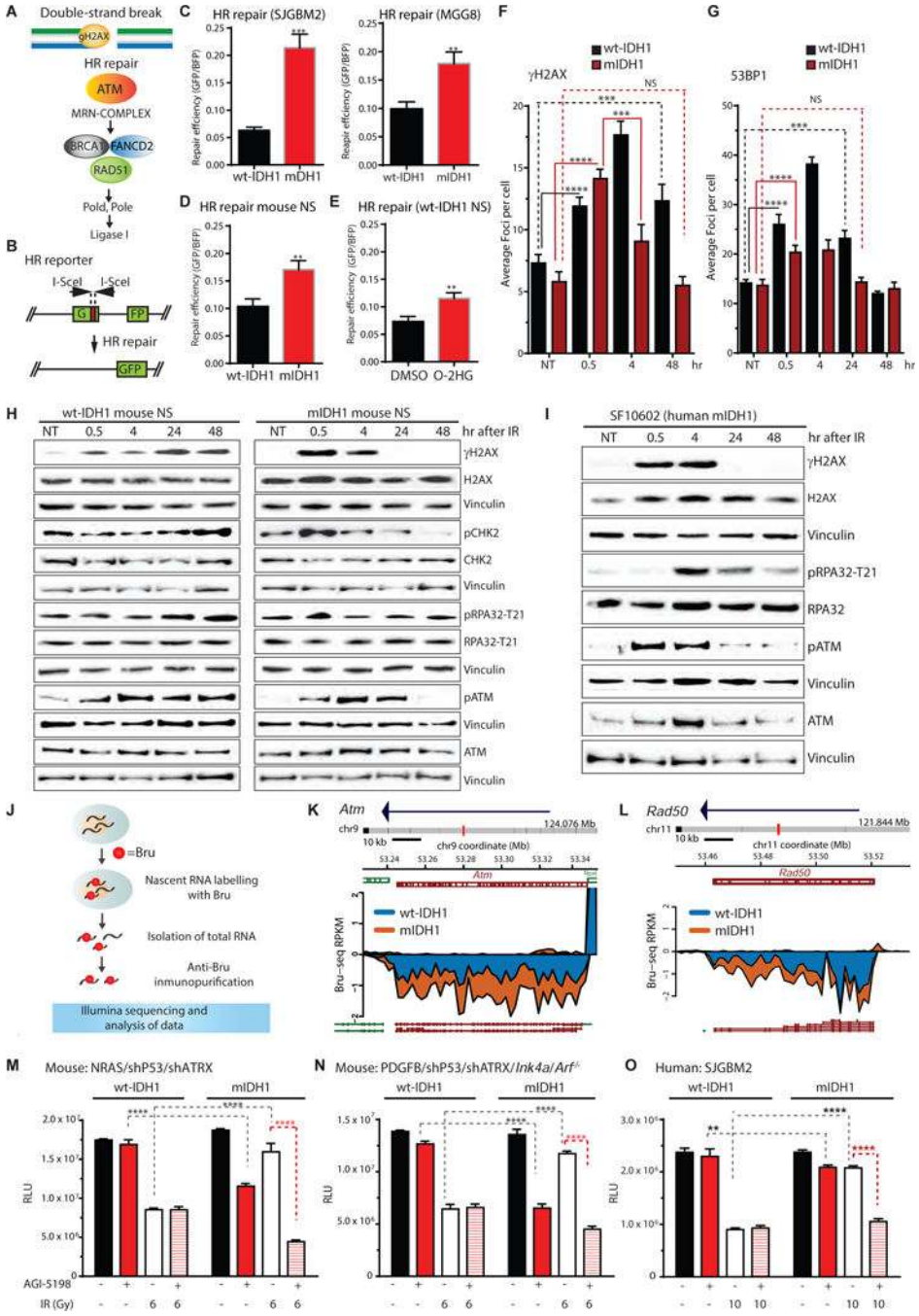

Figure 4. IDH1^{R132H} enhances DNA repair efficiency and confers in vitro radioresistance.

(**A**) Diagram of HR repair pathway.

(**B**) HR repair reporter assay. Diagram shows the HR reporter plasmid and the mechanism to measure HR repair efficiency by reconstitution of GFP expression.

(**C-E**) Bar graphs show HR repair efficiency in wt-IDH1 and mIDH1 human glioma cells (C); wt-IDH1-NS and mIDH1-NS (D); and in wt-IDH1-NS treated with O-2HG (E). GFP expression was normalized by blue fluorescent protein expression (BFP). **p < 0.01; ***p < 0.001; unpaired t- test (n = 3 technical replicates).

Author Manuscript Author Manuscript Author Manuscript Author Manuscript

(**F**) Quantification of γH2AX foci in wt-IDH1-NS and mIDH1-NS from 0 to 48 hours after 2 Gy IR (Fig. S9). Bar graph represents the average number of foci per nuclei. ***p < 0.001; ****p < 0.0001; one-way ANOVA (n = 3 technical replicates).

(**G**) Quantification of 53BP1 foci in wt-IDH1-NS and mIDH1-NS from 0 to 48 hours after 2 Gy IR. Bar graph represents the average number of foci per nuclei. ***p < 0.001; ****p < 0.001 oneway ANOVA (n = 3 technical replicates).

(**H**) WB shows γH2AX, pCHK2, pRPA32, pATM levels, and non-phosphorylated proteins respectively from 0 to 48 hours after 2 Gy. Vinculin: loading control.

(**I**) WB shows γH2AX, pRPA32 and pATM amounts from 0 to 48 hours after 20 Gy of IR. Vinculin: loading control.

(**J**) Diagram of Bru-seq assay to identify nascent RNAs labeled with bromouridine (Bru).

(**K, L**) Bru-seq traces show differential transcriptional rates ($p < 0.05$; fold-change < 1.5) of DNA repair genes *Atm* (K) and *Rad50* (L) in mIDH1-NS (orange) compared to wt-IDH1-NS (blue). Arrows indicate sequence strand reading direction. Genes shown on top in red indicate minus strand genes. The gene maps were generated from RefSeq. Genes and chromosome locations are indicated on the maps. Data is expressed in reads per kilobase per million mapped reads (RPKM).

(**M-O**) Impact of mIDH1 on radiosensitivity in NS: NRAS/shP53/shATRX (M), PDGFB/shP53/shATRX/*Ink4a/4rf*$^{-/-}$ (N), and human glioma cells SJGBM2 (O). Cell viability assay shows the effect of AGI-5198 +/- IR on cell proliferation in wt-IDH1 and mIDH1 human glioma cells. Results are expressed in relative luminescence units (RLU). *p < 0.05; **p < 0.01; ****p < 0.0001; two-way ANOVA (n = 3 technical replicates).

Author Manuscript Author Manuscript Author Manuscript Author Manuscript

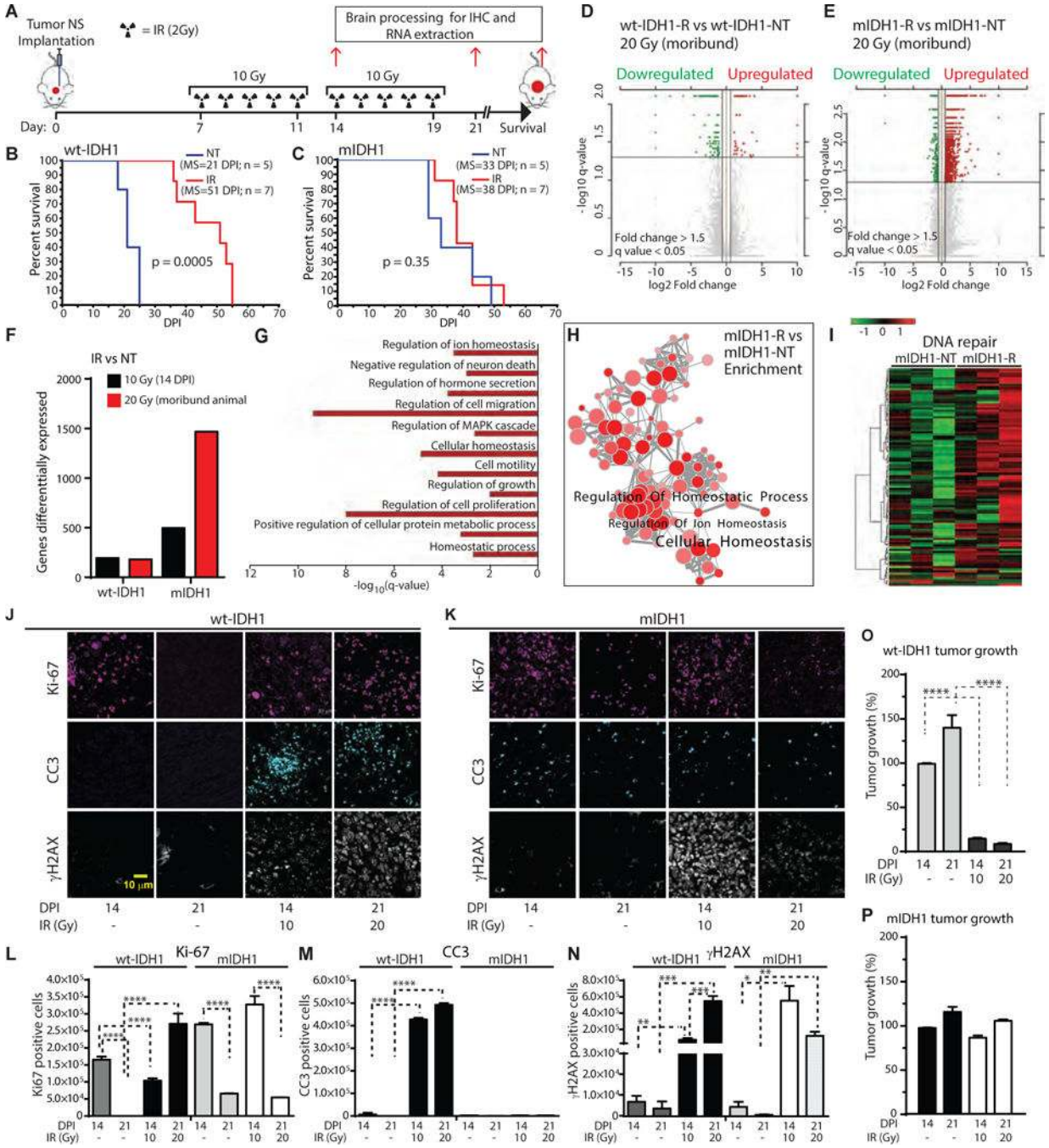

Figure 5. IDH1^{R132H} confers in vivo radioresistance

(**A**) Pre-clinical trial design for testing the role of mIDHI on radio-response in an orthotopic mIDHI glioma model. Mutant IDH1-NS and wt-IDHl-NS were implanted into adult mice (day 0). 7 days post-implantation (DPI) animals were split into 6 groups: i) 2 Gy/day/5 days (total=10 Gy), euthanized at 14 DPI (n=7); ii) no treatment group (NT), euthanized at 14 DPI (n=5); iii) 2 Gy/day/10 days (total=20 Gy), euthanized at 21 DPI (n=7); iv) NT, euthanized at 21 DPI (n=5); v) 2 Gy/day/10 days (total=20 Gy), euthanized at moribund stage (MS = 51 DPI for wt-IDH1 and 38 DPI for mIDH1 tumor-bearing mice) (n=7); and,

Author Manuscript Author Manuscript Author Manuscript Author Manuscript

vi) NT, euthanized at moribund stage (n=5) (MS = 21 DPI for wt-IDH1 and 33 DPI for mIDH1 tumor-bearing mice). Tumors were processed for immunohistochemistry and RNA-seq analysis.

(**B-C**) Kaplan-Meier survival curve of wt-IDH1 (B) and mIDH1 (C) tumor-bearing mice treated with 20 Gy (n = 7) or NT (n = 5). Statistical significance was determined by Mantel-Cox test.

(**D**) Volcano plot showing the comparison of gene expression in wt-IDH1 tumors from mice treated with 20 Gy, and processed at moribund stage (wt-IDH1-R) versus untreated wt-IDH1 tumors (wt-IDH1-NT). The -log10 q-values were plotted against the log2 (FC). Upregulated genes (n = 55; ≥1.5-fold; FDR corrected p-value < 0.05) are depicted as red dots, genes that were downregulated (n = 149; FDR ≥1.5-fold, corrected p-value < 0.05) are depicted as green dots. FDR corrected p-values = q-values; two-sided moderated Student's t-test.

(**E**) Volcano plot showing the comparison of gene expression in mIDH1 tumors from mice treated with 20 Gy, and processed at moribund stage (mIDH1-R) versus control mIDH1 tumors that were not treated (mIDH1-NT). The -log10 q-values were plotted against the log2 (FC). Upregulated genes (n = 1295; ≥1.5-fold; FDR corrected p-value < 0.05) are depicted as red dots, genes that were downregulated (n = 184; ≥1.5-fold; FDR corrected p-value < 0.05) are depicted as green dots. FDR corrected p-values = q-values; two-sided moderated Student's t-test.

(**F**) Bar graph showing the total number of DE genes (fold-change ≥1.5; q < 0.05) in wt-IDH1 (wt-IDH1-R versus wt-IDH1-NT) and mIDH1 (mIDH1-R versus mIDH1-NT) gliomas after 10 or 20 Gy.

(**G**) Functional enrichment of DE genes in mIDH1-R group.

(**H**) Pathway enrichment map from GSEA of mIDH1-R tumors versus mIDH1-NT tumors. Red nodes illustrate differential enrichment (upregulation) in mIDH1-R tumors (p < 0.05, overlap cutoff >0.5).

(**I**) Heat-map showing gene expression pattern for DNA repair genes in mIDH1-NT and mIDH1-R tumors treated with 20 Gy (n = 3 biological replicates). Differentially upregulated genes are depicted in red, whereas downregulated genes are depicted in green (FDR ≤0.05; fold-change ≥± 1.5).

(**J-K**) Immunofluorescence staining of Ki-67, CC3 and γH2AX in wt-IDH1 (J) and mIDH1 (K) mice at 14 and 21 DPI +/− IR treatment at the indicated doses. Scale bar = 10μm.

(**L-N**) Quantification of immunofluorescence staining. Bar graphs represent total numbers of cells positive for Ki-67 (L), CC3 (M) and γH2AX (N). *p < 0.05; **p < 0.01; ***p < 0.001; ****p < 0.0001; unpaired t-test. Data shown as ± SEM (n = 3 biological replicates).

(**O-P**) Tumor progression was evaluated by tumor size quantification of wt-IDH1 (O) and mIDH1 (P) tumor sections at 14 and 21 DPI with or without mIDH1 IR treatment at the indicated doses. Tumor size is expressed as percent relative to untreated tumors at 14 or 21 DPI (100%).

Author Manuscript Author Manuscript Author Manuscript Author Manuscript

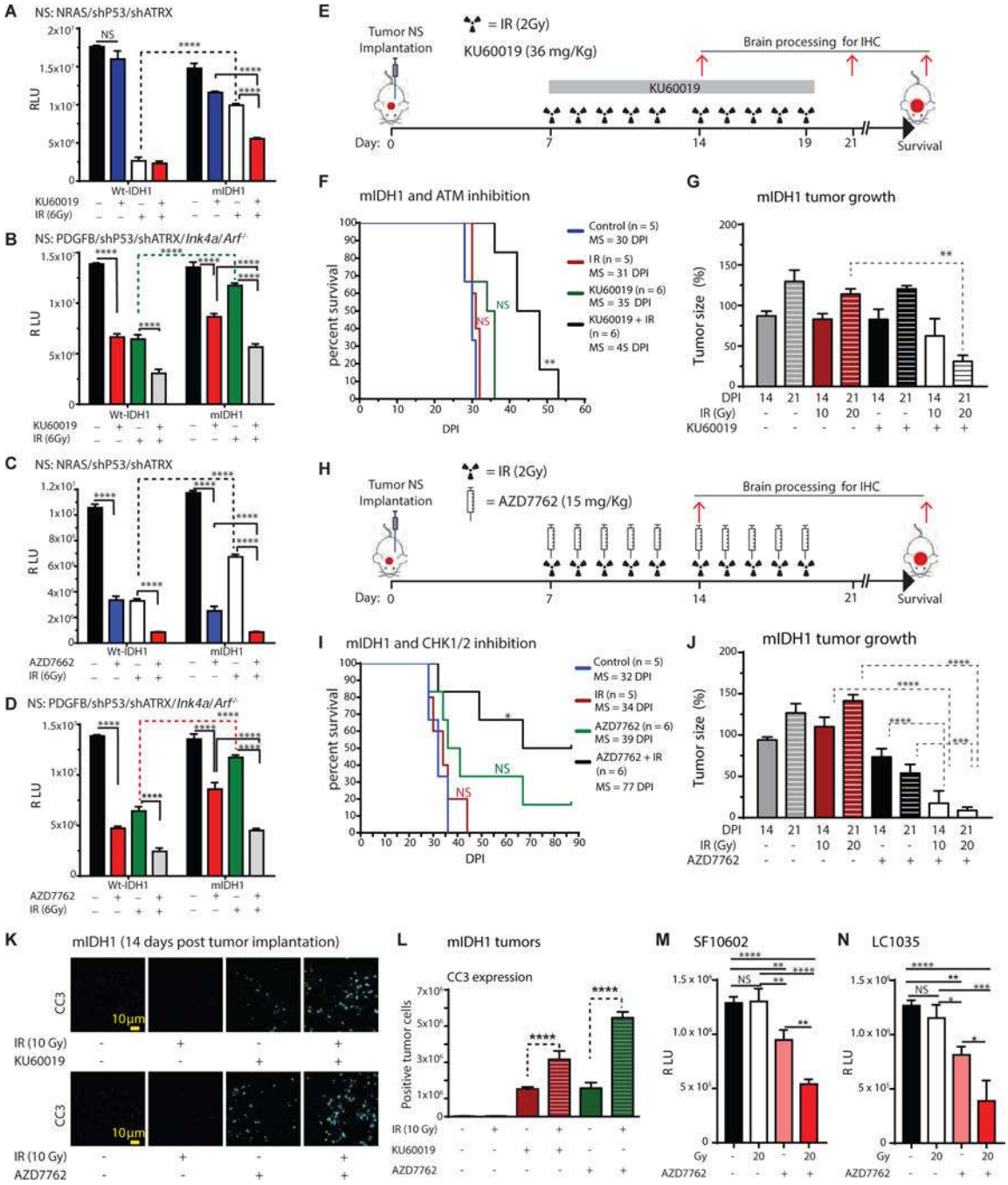

Figure 6. Inhibition of DDR reverts in vivo radioresistance in mIDH1 glioma.

(**A-B**) Inhibition of ATM pathway in mouse glioma cells expressing mIDH1. In vitro data showing cell proliferation of mouse NS: NRAS/shP53/shATRX (A) and PDGFB/shP53/shATRX/*Ink4a/Arf*$^{-/-}$ (B), +/- mIDH1, in response to 6 Gy combined with or without 1.5μM of KU60019. ****p < 0.0001; two-way ANOVA. Non-significant = NS. Data shown as mean ± SEM (n = 3 technical replicates).

(**C, D**) Inhibition of CHK1/2 in mouse mIDH1-NS. In vitro data showing cell proliferation of mouse NS: NRAS/shP53/shATRX (C) and PDGFB/shP53/shATRX/*Ink4a/Arf*$^{-/-}$ (D), with

Author Manuscript Author Manuscript Author Manuscript Author Manuscript

or without mIDH1, in response to 6 Gy combined with 1.5μM of AZD7762. ****p < 0.0001; two-way ANOVA. Non-significant = NS. Data shown as mean ± SEM (n = 3 technical replicates).

(**E**) Pre-clinical trial design for testing the impact of the ATM inhibitor (KU60019) on the response to IR in an orthotopic glioma model. 7 days post NS implantation (DPI), animals were separated into 8 groups: i) untreated (NT) euthanized at 14 DPI; ii) IR 2 Gy/day/5 days (total = 10 Gy), euthanized at 14 DPI; iii) KU60019 (continuous infusion for 5 days; 36 mg/kg/day), euthanized at 14 DPI; iv) KU60019 (continuous infusion for 5 days; 36 mg/kg/day) plus 2 Gy/day/5 days (total= 10 Gy), euthanized at 14 DPI; v) NT, euthanized at moribund stage (between 30 to 50 DPI); vi) 2 Gy/day/10 days (total= 20 Gy), euthanized at moribund stage; vii) KU60019 (continuous infusion for 10 days; 36 mg/Kg/day), euthanized at moribund stage; and viii) KU60019 (continuous infusion for 10 days; 36 mg/Kg/day) plus 2 Gy/day/10 days (total= 20 Gy), euthanized at moribund stage.

(**F**) Kaplan-Meier survival curve of mIDH1 tumor-bearing mice treated with +/- 20 Gy (n = 5) in the presence or absence of KU60019 (n = 6). **p < 0.01; Mantel-Cox test.

(**G**) Analysis of tumor progression evaluated by tumor size of mIDH1 glioma sections at 14 and 21 DPI +/- IR at the indicated doses in the presence or absence of KU60019. Tumor size was expressed as percentage relative to untreated tumors at 14 or 21 DPI (100%).

(**H**) Trial design for testing the impact of CHK1/2-signaling inhibitor (AZD7762) on the response to IR in an orthotopic glioma model. 7 days post-implantation (DPI) of NS, the animals were separated into 8 groups as described in (E), but treated with AZD7762 (15 mg/kg/day).

(**I**) Kaplan-Meier survival curve of mIDH1 bearing mice +/- 20Gy (n=5), in combination with AZD7762 (15 mg/kg/day) (n = 6). MS of mice bearing mIDH1 tumors was significantly increased after IR combined with AZD7762 (*p < 0.01; Mantel-Cox test).

(**J**) Analysis of tumor size evaluated by quantification of mIDH1 brain tumor sections at 14 DPI +/− IR at the indicated doses, in the presence or absence of AZD7762. Tumor size is expressed as percentage relative to untreated tumors at 14 or 21 DPI (100%).

(**K**) Immunofluorescence staining of CC3 expression at 14 DPI +/- IR treatment at the indicated doses, in the presence or absence of KU60019 or AZD7762. Scale bar = 10μm.

(**L**) Bar graphs represent total numbers of CC3+ cells (K panel). ****p < 0.0001; unpaired t-test. Data shown as mean ± SEM.

(**M-N**) Impact of CHK1/2 inhibition on radioresistance in human glioma cells with endogenous expression of mIDH1: SF10602 (M) and LC1035 (N). Cell viability assay shows the effect of AZD7762. The results are expressed in relative luminescence units (RLU). **p < 0.01; ****p < 0.0001; two-way ANOVA.Supplementary Materials